Original Article

Variability of radiomic features extracted from multi-b-value diffusion-weighted images in hepatocellular carcinoma

Jing Zhang[1,2#], Qingtao Qiu[1#], Jinghao Duan[1], Guanzhong Gong[1], Qingjun Jiang[3], Gang Sun[3], Yong Yin[1]

[1]Department of Radiation Oncology, Shandong Cancer Hospital Affiliated to Shandong University, Shandong Academy of Medical Sciences, Ji'nan 250117, China; [2]Shandong Province Key Laboratory of Medical Physics and Image Processing Technology, Institute of Biomedical Sciences, School of Physics and Electronics, Shandong Normal University, Ji'nan 250358, China; [3]Department of Medical Imaging, Jinan Military General Hospital, Ji'nan 250031, China

Contributions: (I) Conception and design: J Duan, Y Yin; (II) Administrative support: Y Yin; (III) Provision of study materials or patients: Q Jiang, G Sun; (IV) Collection and assembly of data: J Zhang, Q Qiu, G Gong; (V) Data analysis and interpretation: J Zhang, Q Qiu, J Duan; (VI) Manuscript writing: All authors; (VII) Final approval of manuscript: All authors.

[#]These authors contributed equally to this work.

Correspondence to: Yong Yin; Jinghao Duan. Department of Radiation Oncology, Shandong Cancer Hospital Affiliated to Shandong University, Shandong Academy of Medical Sciences, Ji'nan 250117, China. Email: yinyongsd@126.com; jinghaoduan@126.com.

Background: Reliable and meaningful radiomic features is extremely crucial to characterize tumor phenotypes. This study was designed to experimentally evaluate the variability of radiomic features extracted from different b-values diffusion-weighted images (DWIs) in hepatocellular carcinoma (HCC).

Methods: The research population was composed of 34 HCC patients and 12 healthy volunteers. At 3.0T MR scanner, with the identical imaging protocols, all cases underwent the following sequences at 10 b-values ranging from 0 to 1,500 s/mm^2: T1WI, T2WI, multiple phases contrast-enhanced and intravoxel incoherent motion-DWI scans. For HCC trail, gross tumor volume (GTV) were manually delineated by an experienced radiologist at the b=0 s/mm^2 DWI sequence. For healthy volunteers trail, 3 cylindric regions of interest (ROIs) with 14 mm in height and approximately 20 mm in diameter were defined in parenchyma at II/III, V/VI and VII hepatic segments. Using 3D Slicer Radiomics software (www.slicer.org), we extracted 74 radiomic features, including 19 first-order statistical features and 55 texture features for each case sequence. Percentage coefficient of variation (%COV) was applied to evaluate the stability of each feature and %COV <30 was considered as low variation. Furthermore, to observe the trend for radiomic features value in various b-values DWIs, an exponential or polynomial model was used. Finally, concordance correlation coefficient (CCC) was applied to assess the reproducibility of radiomic features between different b-values DWIs.

Results: The value of intensity histogram features and texture features derived from DWIs showed a dependency on the b-values in HCC. The low variations (%COV <30), moderate variations (30≤ %COV <50) and large variations (%COV ≥50) radiomic features accounted for about 26%, 28%, and 46%, respectively. The exponential and polynomial model indicated that about 70% radiomic features showed positive or negative dependence on b-values and about 4% radiomic features showed little dependence. We acquired a better fitting results in HCC group (the mean value and standard deviation of R-square were 0.958±0.096 and 0.896±0.071, P<0.05). Moreover, we found radiomic features extracted from nearby b-values (b=0, 20, 50, 100, 200 s/mm^2 and b=1,000 s/mm^2) of DWIs showed a high reproducibility. Twelve radiomic features can be used to identify HCC and normal liver.

Conclusions: Being influenced by different b-values, radiomic features tested here exist variability in HCC DWIs. Most features are unstable and extremely dependent on b-values in DWIs. Meanwhile, the research revealed that reproducible features can be extracted by nearby b-values DWIs.

Keywords: Hepatocellular carcinoma (HCC); diffusion-weighted imaging (DWI); radiomic features

Submitted Sep 28, 2018. Accepted for publication Jan 07, 2019.
doi: 10.21037/tcr.2019.01.14
View this article at: http://dx.doi.org/10.21037/tcr.2019.01.14

Introduction

Hepatocellular carcinoma (HCC) is one of the most common malignant tumors in China (1) and the third leading cause of cancer to death worldwide (2). The diagnosis and assessments for HCC are benefited much from the existing medical imaging techniques, such as ultrasound, CT, MRI and PET. Liver biopsy is considered as the golden standard for the assessment of hepatic diseases, although it is invasive and easily affected by the sampling error (3). It is a hot topic to find a reproducible and repeatable method to assist the diagnosis of malignancy.

Medical imaging plays a crucial role in the diagnosis and identification of the HCC (4). 3.0T MR is recognized to be better than 1.5T MR and CT in characterizing soft tissue (5) or solid organ tumors (6,7). However, the MR images quality are affected by many factors, such as tissue cellularity, vascularity, necrosis and the respiratory movements, etc. It is not an easy task to decipher different MRI sequences (or parameters) for inexperienced radiologists. Radiomics is an emerging field in quantitative imaging that uses high-dimensional imaging features to objectively and quantitatively describe tumour phenotypes (8,9). Recent studies have reported that radiomic features extracted from multiple sequences MR images can be used for diagnostics (10), predicting treatment response (11) and histological grade (12) in HCC. Meanwhile, radiomics can characterize intratumour heterogeneity and can be served as a biomarkers of tumor (13). However, radiomics features are sensitive to noise and imaging protocols (14).

Diffusion weighted images (DWIs) and apparent diffusion coefficient (ADC) values with multiple b-values are often used to assist qualitative and quantitative diagnosis of malignancy from benign tumors (15,16). Radiomic features extracted from DWIs showed a good accuracy in distinguishing benign and malignant ovarian lesions (17) and appear useful for prostate cancer detection and Gleason scores (GS) assessment (18). As yet, there was no widely-accepted standardized algorithm about the b-value in HCC DW imaging, as it is easily affected by many factors. Vascular perfusion can increase the sensibility of HCC at low b-value DWI (19). Nevertheless, high b-value DWI showed a good specificity of dysplastic nodules of HCC (20), although signal to noise ratio (SNR) will decrease in high b-value (21). Therefore, due to the lack of any standardized MR imaging parameters, variability may be inevitable in DWI radiomic features of HCC.

The aim of this study was to experimentally investigate the variability of radiomic features extracted from multi-b-values DWIs in HCC and explore stable radiomic features to characterize HCC.

Methods

Patient group

Informed consent was obtained from all patients, and Jinan Military General Hospital Ethics committee approved the study protocol (No: 2015-353). Fifty candidates with HCC and 12 healthy volunteers were randomly selected in this study between January 2016 and December 2017 in Jinan Military General Hospital. All cases experienced the following MR sequences scans: T1-weighted imaging (T1WI), T2-weighted imaging (T2WI), Gd-DTPA contrast-enhanced and intravoxel incoherent motion-diffusion weighted imaging-echo planar imaging (IVIM-DWI-EPI). All HCC patients were diagnosed by experienced radiologists and proved by pathology. Eligibility criteria were as follows: (I) cases were diagnosed with HCC by three radiologists; (II) at least two slices showed visible lesions. Exclusion criteria were as follows: (I) have experienced chemoradiotherapy, surgical resection or other treatment; (II) images artifacts; (III) data partial missing; (IV) ascites; (V) liver cancer metastasis. Finally, 34 HCC patients (23 males and 11 females aged from 42 to 84 years with mean age 59.8 years) and 12 healthy volunteers (7 males and 5 females aged from 31 to 78 years, with mean age 54.6 years) were included in this study.

Image acquisition

Before scanning, all cases underwent a bolus injection of

0.02 mmol/kg body weight Gd-DTPA (Primovist, Bayer-Schering Pharma, Berlin, Germany) at a rate of 2.5 mL/s and immediately followed by a 15 mL saline flush. Every person was scanned on 3.0T scanner (GE 3.0T Discovery MR 750) using an eight-channel phase array coil. The MR sequences parameters were as follows: (I) axial T1WI: repetition time (TR) =3.7 ms, echo time (TE) =1.7 ms, slice thickness =5.2 mm, interslice gap =−2.6 mm and NEX =0.7; (II) axial T2WI: TR =6,667 ms, TE=1.7 ms, interslice gap = 1 mm and NEX =2.5; (III) IVIM-DWI-EPI: TR =5,714 ms, TE =66.1 ms, slice thickness =7 mm, interslice gap =1 mm, NEX =2, MB =10 (b-values: 0, 20, 50, 100, 200, 400, 800, 1,000, 1,200, 1,500 s/mm^2); (IV) axial contrast-enhanced imaging (TR =3.7 ms, TE =1.7 ms, interslice gap =−2.6 mm and NEX =0.7) and coronal contrast-enhanced imaging (TR =3.6 ms, TE =1.7 ms, interslice gap =−2.0 mm and NEX =0.7).

Volume of interests (VOIs) segmentation

VOIs were delineated manually by one radiologist with 20 years experiences in MIM software (www.mimsoftware.com): (I) for HCC trail, the expert delineated gross tumor volume (GTV) on the first DWI sequence (b=0 s/mm^2) referenced by T1WI, T2WI and contrast-enhanced imaging sequence; (II) for healthy volunteer trail, avoiding great vessels, 3 VOIs with 14 mm in height and approximately 20 mm in diameter were defined in parenchyma at II/III, V/VI and VII hepatic segments; (III) VOIs in DWI (b=0 s/mm^2) were mapped to the rest 9 b-values DWI using function clone in the MIM software.

Extraction of Radiomic features

Radiomic features were automatically calculated using 3D Slicer Radiomics software (www.slicer.org), which was an open-source software platform for medical image informatics, image processing, and three-dimensional visualization. Totally, we extracted 74 radiomic features for each case sequence. The radiomic features were divided into four groups: (I) 19 first-order intensity histogram (IH) features; (II) 23 gray-level co-occurrence matrix (GLCM) features; (III) 16 gray-level run-length matrix (GLRLM) features; (IV) 16 gray-level size-zone matrix (GLSZM) features. Detailed mathematical descriptions of these radiomic features can be found in reference (13).

Data analysis

Firstly, mean value (mean) and standard deviation (SD) for each feature were calculated across ten b-values DWIs. Then, to evaluate the variability of the features, percentage coefficient of variation (%COV) was calculated for each radiomic feature in this paper. %COV <30 was considered as low variation, 30≤ %COV <50 was considered as moderate variations and %COV ≥50 was considered as large variations. The definition of %COV (22) was as follows:

$$\%\mathrm{COV} = \frac{S.D}{Mean} \times 100$$

Secondly, using exponential model or polynomial fit model, graphs were drawn for each feature and different b-values. The equations were as follows:

$$F = F_0 e^{-cb} + k$$
$$F = F_0 e^{cb} + k$$

F is the feature value, F_0 is the feature value at b=0 s/mm^2, and c is the decay or growth constant. R-square ≥0.9 was considered a better fitting degree. Spearman correlation coefficient (r) between b-value and radiomic feature value was computed for each graph. We adopted Karlik's quoted guidelines for interpretation for the correlation measures (23).

If the absolute value of r (|r|) was

(I) Less than 0.2—negligible correlation;
(II) Between 0.2 and 0.4—weak correlation;
(III) Between 0.4 and 0.7—moderate correlation;
(IV) Between 0.7 and 0.9—strong correlation;
(V) Between 0.9 and 1—very strong correlation.

Thirdly, concordance correlation coefficient (CCC) was applied to evaluate the reproducibility of radiomic features between nearby b-values DWIs. The definition of CCC (24,25) is as follows:

$$\mathrm{CCC} = \frac{2\rho\sigma_x\sigma_y}{\sigma_x^2 + \sigma_y^2 + \left(\mu_x - \mu_y\right)^2}$$

where x and y are the vector of radiomic feature values derived from two b-value DWIs, ρ, σ and μ are correlation coefficient, standard deviation and mean value of vector x and y, respectively. CCC value ≥0.8 was considered as reproducible.

Finally, statistical analysis was performed using SPSS software 22.0 (SPSS, Chicago, IL, USA). Independent-sample t-test was used to compare the differences of

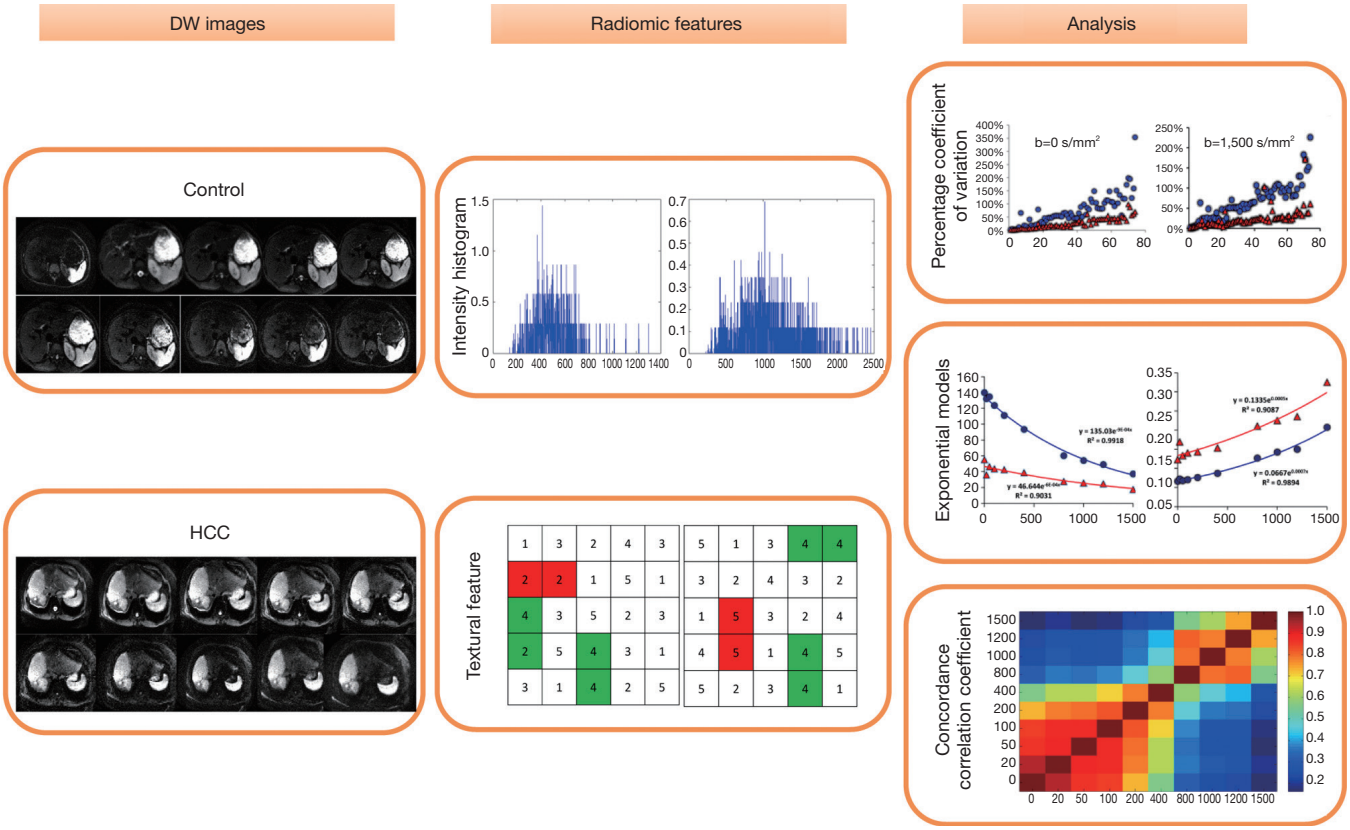

Figure 1 Flow chart of this study.

%COV between two groups. Paired Student's *t*-tests or Wilcoxon rank tests were used to compare the differences of CCC between different b-values. P<0.05 was considered statistically significant. The flow chart of this study was depicted in *Figure 1*.

Results

Variation of radiomic features

The name of feature index was consistent in *Figure 2* and in *Table 1*. *Figure 2* demonstrated the %COV value of each radiomic feature in HCC group and control group. In HCC group, 26% features showed low variations (%COV <30), including 2 IH features, 7 GLCM features, 6 GLRLM features and 4 GLSZM features. Twenty-eight percent features showed moderate variations (30≤ %COV <50), including 11 IH features, 6 GLCM features, 2 GLRLM features and 2 GLSZM features. Forty-six percent features showed large variations (%COV ≥50), including 6 IH features, 10 GLCM features, 8 GLRLM features and 10 GLSZM features. In IH feature group, 17 (89%) features showed moderate or large variations, and 2 (11%) features showed low variations. In GLCM

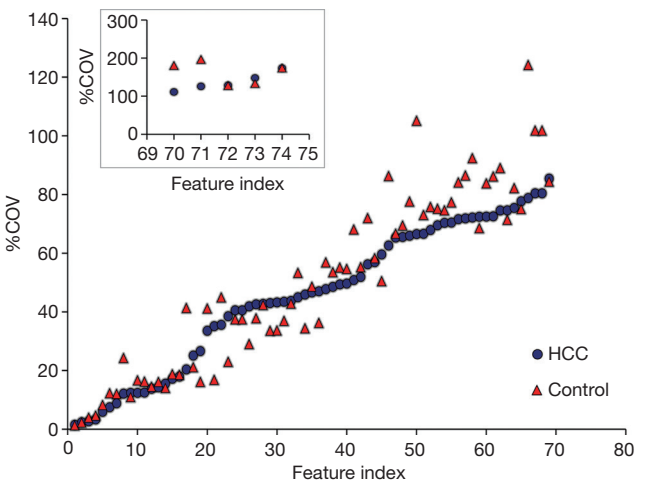

Figure 2 The %COV absolute value of each radiomic feature across 10 b-values DW image sets.

Table 1 Groups of 74 radiomic features based on %COV value

Low (%COV <30)
1-GLCM-IDMN
2-GLCM-IDN
3-GLRLM-SRE
4-GLRLM-R.Percent
5-GLRLM-RLNUN
6-GLSZM-Z.Entropy
7-GLRLM-RLNU
8-GLCM-IMC2
9-GLCM-Entropy
10-GLRLM-R.Entropy
11-GLRLM-LRE
12-GLSZM-GLNU
13-GLCM-SumEntropy
14-GLSZM-SAE
15-IH-Entropy
16-GLCM-DiffEntropy
17-IH-Kurtosis
18-GLSZM-SZNUN
19-GLCM-ID
Moderate (%COV <50)
20-GLSZM-Z.Percent
21-GLCM-InverseVar
22-GLCM-IMC1
23-GLCM-IDM
24-GLCM-AverInten
25-GLCM-SumAver
26-GLRLM-GLNU
27-IH-MeanAbsDev
28-IH-StandDev
29-IH-RobustAbsDev
30-IH-InterQuarRange
31-GLCM-DiffAver
32-GLSZM-GLNUN
33-IH-Range
34-GLRLM-GLNUN
35-IH-90Percentile
36-IH-Uniformity
37-IH-Maximum
38-IH-RootMeanSqua
39-IH-Mean
40-IH-Median
Large (%COV >50)
41-GLSZM-LAHGLE
42-GLSZM-SZNU
43-IH-10Percentile
44-GLCM-MaxProbablity
45-GLRLM-R.Var
46-GLCM-Correlation
47-GLRLM-LRHGLE
48-GLCM-Energy
49-GLSZM-GL.Var
50-IH-Skewness
51-GLSZM-SALGLE
52-GLSZM-HGLZE
53-GLRLM-HGLRE
54-GLCM-AutoCorre
55-GLRLM-SRHGLE
56-GLRLM-GL.Var
57-GLCM-ClusTend
58-GLCM-DiffVar
59-GLRLM-SRLGLE
60-GLCM-SumSqua
61-IH-Variance
62-GLSZM-SAHGLE
63-GLRLM-LGLRE
64-GLCM-Contrast
65-GLSZM-LGLZE
66-IH-Minimum
67-IH-TotalEnergy
68-IH-Energy
69-GLRLM-LRLGLE
70-GLCM-ClusProm
71-GLCM-ClusShade
72-GLSZM-LAE
73-GLSZM-Z.Var
74-GLSZM-LALGLE

Table 1 (*continued*)

Table 1 (*continued*)

Table 2 The mean value of 18 radiomic features which shows low variations in HCC and control groups

Feature	HCC		Control		P
	Mean	SD	Mean	SD	
1-GLCM-IDMN	0.951	0.003	0.955	0.005	0.200
2-GLCM-IDN	0.860	0.004	0.865	0.009	0.662
3-GLRLM-SRE	0.946	0.024	0.905	0.033	<0.001
4-GLRLM-R.Percent	0.931	0.030	0.882	0.375	<0.001
5-GLRLM-RLNUN	0.877	0.049	0.789	0.059	<0.001
6-GLSZM-Z.Entropy	5.179	0.375	4.622	0.499	<0.001
7-GLRLM-RLNU	219.213	18.645	181.472	19.906	<0.001
8-GLCM-IMC2	0.864	0.095	0.615	0.126	<0.001
9-GLCM-Entropy	6.233	0.744	5.156	0.787	<0.001
10-GLRLM-R.Entropy	4.084	0.507	3.293	0.324	0.025
11-GLRLM-LRE	1.285	0.166	1.499	0.233	0.019
12-GLSZM-GLNU	7.020	0.481	7.377	0.577	0.459
13-GLCM-SumEntropy	4.112	0.567	3.235	0.468	0.059
14-GLSZM-SAE	0.633	0.082	0.529	0.033	0.145
15-IH-Entropy	3.772	0.637	2.741	0.466	0.148
16-GLCM-DiffEntropy	3.075	0.540	2.344	0.391	0.563
18-GLSZM-SZNUN	0.397	0.084	0.283	0.025	0.001
19-GLCM-ID	0.355	0.085	0.485	0.072	<0.001

HCC, hepatocellular carcinoma.

feature group, 16 (70%) features showed moderate or large variations, and 7 (30%) features showed low variations. In GLRLM feature group, 10 (62%) features showed moderate or large variations, and 6 (38%) features showed low variations. In GLSZM feature group, 12 (75%) features showed moderate or large variations, and 4 (25%) features showed low variations. In control group, 28% features showed low variations (%COV <30), including 1 IH features, 9 GLCM features, 7 GLRLM features and 4 GLSZM features. Nineteen percent features showed moderate variations (30≤ %COV <50), including 8 IH features, 3 GLCM features, 1 GLRLM features and 2 GLSZM features. Fifty-three percent features showed large variations (%COV ≥50), including 10 IH features, 11 GLCM features, 8 GLRLM features and 10 GLSZM features. In IH feature group, 18 (95%) features showed moderate or large variations, and 1 (5%) features showed low variations. In GLCM feature group, 14 (61%) features showed moderate or large variations, and 9 (39%) features showed low variations. In GLRLM feature group, 9 (56%) features showed moderate or large variations, and 7 (44%) features showed low variations. In GLSZM feature group, 12 (75%) features showed moderate or large variations, and 4 (25%) features showed low variations. The intersection of low variation features was 18 (24%) in the two sets and the mean value of each feature was listed in *Table 2*. Among them, 12 (16%) radiomic features showed a statistically significant difference between HCC group and control group.

Influence of b-value

Table 3 provided the fitting degree for two sets. For HCC and control group, 66 (89%) and 48 (65%) features obtained a better fitting degree, respectively. Among them, the number of better fitting features in IH feature group, GLCM feature group, GLRLM feature group and GLSZM feature group was 17 (23%), 19 (26%), 16 (22%) and 14

Table 3 R^2 and r value of fitting results between each feature and different b-values

Feature	Control		HCC	
	R^2	r	R^2	r
1	0.74	−0.50	0.6	−0.10
2	0.87	−0.38	0.76	−0.07
3	0.86	−0.74	0.95	−0.67
4	0.86	−0.73	0.95	−0.67
5	0.87	−0.73	0.96	−0.67
6	0.92	−0.81	0.98	−0.49
7	0.87	−0.72	0.97	−0.20
8	0.95	−0.83	0.98	−0.62
9	0.9	−0.79	0.98	−0.50
10	0.92	−0.83	0.99	−0.60
11	0.84	0.73	0.93	0.66
12	0.61	−0.33	0.85	0.1
13	0.92	−0.82	0.99	−0.55
14	0.9	−0.57	0.98	−0.63
15	0.91	−0.81	0.99	−0.63
16	0.89	−0.80	0.99	−0.62
17	0.72	−0.63	0.86	−0.21
18	0.81	−0.56	0.98	−0.64
19	0.88	0.76	0.99	0.65
20	0.9	−0.78	0.98	−0.67
21	0.85	0.77	0.99	0.64
22	0.84	0.81	1	0.59
23	0.88	0.76	0.99	0.65
24	0.94	−0.78	0.99	−0.61
25	0.94	−0.78	0.99	−0.61
26	0.91	0.77	0.99	0.52
27	0.9	−0.81	0.99	−0.55
28	0.92	−0.83	0.99	−0.63
29	0.89	−0.79	0.99	−0.62
30	0.89	−0.79	0.99	−0.61
31	0.81	−0.80	0.99	−0.65
32	0.94	0.82	0.99	0.62
33	0.93	−0.87	0.98	−0.61
34	0.91	0.79	0.99	0.62
35	0.95	−0.85	0.99	−0.64
36	0.91	0.79	0.99	0.62
37	0.93	−0.89	0.98	−0.64
38	0.95	−0.83	0.99	−0.64
39	0.95	−0.82	0.98	−0.63
40	0.95	−0.81	0.99	−0.63
41	0.68	0.55	0.69	0.15
42	0.91	−0.79	0.98	−0.54
43	0.91	−0.77	0.98	−0.60
44	0.9	0.74	0.98	0.55
45	0.86	0.72	0.96	0.65
46	0.84	−0.41	0.72	−0.12
47	0.92	−0.78	0.98	−0.60
48	0.91	0.77	0.97	0.52
49	0.93	−0.85	0.97	−0.62
50	0.5	−0.20	0.38	−0.10
51	0.9	0.82	0.95	0.53
52	0.93	−0.85	0.98	−0.62
53	0.93	−0.80	0.99	−0.62
54	0.93	−0.79	0.98	−0.61
55	0.93	−0.81	0.96	−0.62
56	0.92	−0.84	0.98	−0.63
57	0.92	−0.84	0.98	−0.60
58	0.91	−0.83	0.98	−0.62
59	0.85	0.73	0.98	0.53
60	0.91	−0.83	0.98	−0.62
61	0.92	−0.84	0.99	−0.63
62	0.93	−0.86	0.98	−0.63
63	0.87	0.74	0.98	0.53
64	0.91	−0.81	0.99	−0.64
65	0.93	0.82	0.98	0.57
66	0.81	−0.64	0.96	−0.51
67	0.96	−0.83	0.98	−0.55
68	0.96	−0.83	0.98	−0.55
69	0.91	0.75	0.98	0.55
70	0.9	−0.86	0.96	−0.60
71	0.86	−0.42	0.94	−0.20
72	0.91	0.74	0.96	0.66
73	0.9	0.74	0.97	0.65
74	0.92	0.75	0.92	0.65

R^2 represents R-square; r represents correlation coefficients.

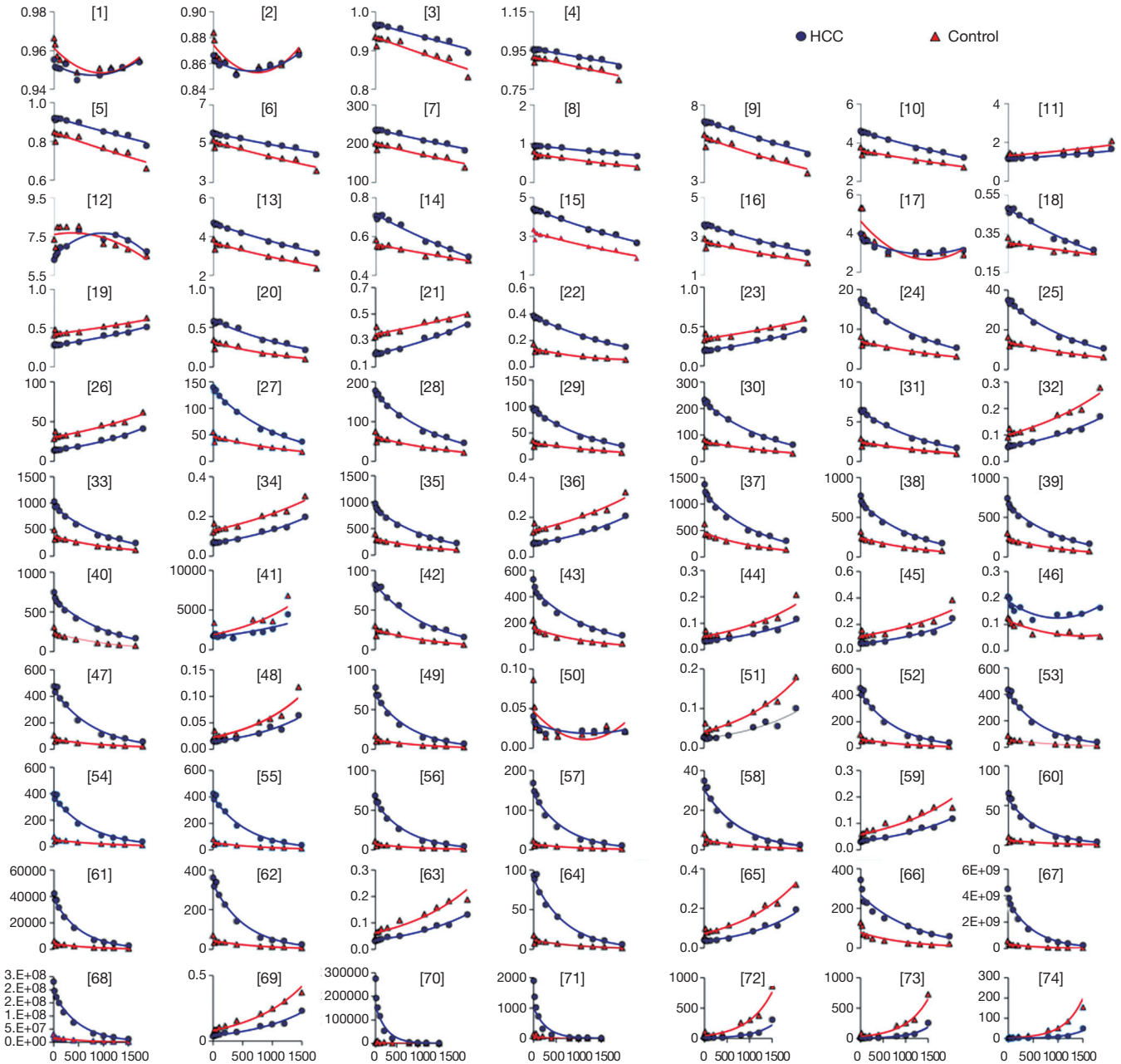

Figure 3 The exponential fitting results or the polynomial fitting results between each feature and different b-values.

(19%) for HCC sets, respectively. The number of better fitting features in IH feature group, GLCM feature group, GLRLM feature group and GLSZM feature group was 14 (19%), 13 (18%), 8 (11%), and 13 (18%) for control sets, respectively. Moreover, the intersection of better fitting features was 47 (64%) in the two sets.

Figure 3 illustrated the exponential fitting results or the polynomial fitting results between each feature and different b-values. The correlation coefficient could be seen in *Table 3*. In HCC group, the number of very strong correlation, strong correlation, moderate correlation, weak correlation and negligible correlation features were 0 (0%), 0 (0%), 65 (88%), 2 (3%) and 7(9%), respectively. The number of positive correlation (r>0.4) and negative correlation (r<–0.4)

Table 4 Correlation analysis results for each feature in four radiomic features groups

Feature group	0.9≤r≤1		0.7≤r<0.9		0.4≤r<0.7		0.2≤r<0.4		<0.2	
	HCC	Con	HCC	Con	HCC	Con	HCC	Con	HCC	Con
IH	0	0	0	16	17	2	1	1	1	0
GLCM	0	0	0	19	19	3	1	1	3	0
GLRLM	0	0	0	16	15	0	0	0	1	0
GLSZM	0	0	0	12	14	3	0	1	2	0

Con represents control group.

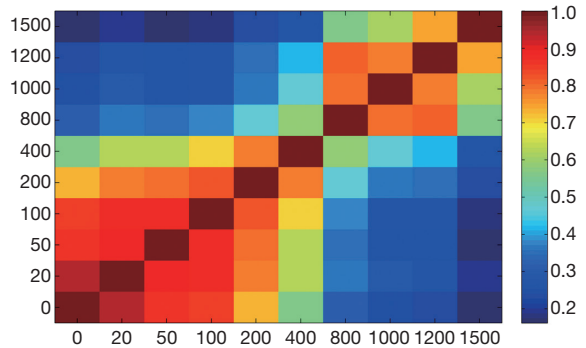

Figure 4 CCC values of radiomic features extracted from nearby b-values DWIs. CCC, concordance correlation coefficient; DWI, diffusion-weighted imaging.

radiomic features were 20 (27%) and 45 (61%) in HCC group, respectively. In control group, the number of very strong correlation, strong correlation, moderate correlation, weak correlation and negligible correlation features were 0 (0%), 63 (85%), 8 (11%), 3 (4%) and 0 (0%), respectively. The number of positive correlation (r>0.4) and negative correlation (r<–0.4) radiomic features were 21 (28%) and 50 (68%), respectively. The correlation analysis results for each feature in four radiomic features groups were listed in *Table 4*.

Reproducibility of radiomic features extracted from nearby b-values DWIs

Figure 4 illustrated that radiomic features extracted from b=0, 20, 50, 100, 200 s/mm^2, and b=1,000 s/mm^2 DWIs acquired high repeatability. Meanwhile, features extracted from nearby b-value DWIs showed high repeatability. Oppositely, features extracted from faraway b-value DWIs usually showed low repeatability.

Discussion

DWIs are generally used to describe the random motion of water molecules. Different histological degree of HCC on the basis of nuclear and structural atypia, high cellular density, cytotoxic edema, and high viscosity can restrict water diffusion. Therefore, most malignant lesions usually show hyperintense in DWIs. DWIs have been widely used in the diagnosis, histopathological grading and prognosis evaluation of abdominal malignant tumor (15,16,26). However, tissue parameters derived from DWIs strongly depend on b-values distributions and organ-specific (19). Due to the variety in MR imaging parameters, variability may be inevitable in imaging biomarker represented by radiomics.

In this study, we demonstrated that the value of radiomic features showed significant correlation with different b-values in DWIs. IH features describe the distribution of voxel intensities. We observed most IH features existed large variation, which indicated that IH features might be strongly influenced by b-value. It was consistent with the previous studies (26,27). In fact, signal intensity of the lesions could enhance along with the increases of b-value in DWIs, which might explain the above phenomenon. Difference with IH features, texture features described statistical interrelationships between voxels with similar contrast values and could provide a measurement of intratumor heterogeneity (22). Density of liver parenchyma, cells geometric arrangements and extracellular matrix in HCC were the most influence factors with the increases of b-values (28). It might result in the phenomenon that most texture features were low variations in different b-value DWIs.

Whether in the HCC group or the control group, we found most radiomic features values had correlation

with the increases of b-value and negative correlation was the main modality. It might be attributed that the signal intensity in the vessel would cause a fast decay with increases of b-values. Besides, most features have similar tendency between two groups (*Figure 3*). Twelve radiomic features had statistically differences between groups and might be used as imaging biomarkers to distinguish HCC and normal liver.

It should be noted that features usually showed high repeatability in nearby b-value DWIs and low repeatability in faraway b-value DWIs (*Figure 4*). Moreover, we also observed reproducible radiomic features in b=1,000 s/mm^2 DWIs. This indicated that nearby b-value DWIs might exist interchangeability in HCC characteristic.

To our knowledge, the reproducibility of MR-based radiomic features has seldom been investigated. Understanding the stability of MR-based radiomic features between different scanning parameters can help identifying reliable features for radiomic applications. In this research, we attempted to detect the impacts of different b-value to radiomic features in HCC DWIs. One limitation of the present study was that we had not employed the ADC maps, which would be added in the future study. Another limitation is that to acquire a reliable result, the noninvasive identification of HCC and healthy liver using imaging biomarker should involve sufficient patient data. In the future work, we will extend the study and seek dependable imaging biomarkers in distinguishing different kinds of liver nodules using radiomic technology.

Conclusions

In this study, we found radiomic features had variability in different b-value DWIs. The value of most features had positive or negative correlation along with the increases of b-value. Features extracted from nearby b-value DWIs usually showed high repeatability. Twelve radiomic features can be used to identify HCC and normal liver.

Acknowledgments

Funding: This research was supported by the Shandong Natural Science Foundation (No. ZR2017PH071) and the WBE Liver Fibrosis Foundation, China (Grant No. CFHPC2019027) and the National Key Research and Development Program of China (No. 2017YFC0113202) and the National Natural Science Fund of China (No. 81472811) and the Key Research and Development Program of Shandong Province (No. 2018GSF118006).

Footnote

Conflicts of Interest: All authors have completed the ICMJE uniform disclosure form (available at http://dx.doi.org/10.21037/tcr.2019.01.14). The authors have no conflicts of interest to declare.

Ethical Statement: The authors are accountable for all aspects of the work in ensuring that questions related to the accuracy or integrity of any part of the work are appropriately investigated and resolved. The study was conducted in accordance with the Declaration of Helsinki (as revised in 2013). Informed consent was obtained from all patients, and Jinan Military General Hospital Ethics committee approved the study protocol (No: 2015-353).

References

1. Wang DF, Chen SD, Zhu GM, et al. Research progress in radiotherapy for hepatocellular carcinoma. Zhonghua Gan Zang Bing Za Zhi 2018;26:238-40.
2. Parkin DM, Bray F, Ferlay J, et al. Estimating the world cancer burden: Globocan 2000. Int J Cancer 2001;94:153-6.
3. Harada TL, Saito K, Araki Y, et al. Prediction of high-stage liver fibrosis using ADC value on diffusion-weighted imaging and quantitative enhancement ratio at the hepatobiliary phase of Gd-EOB-DTPA-enhanced MRI at 1.5 T. Acta Radiol 2018;59:509-16.
4. Ayuso C, Rimola J, Garcia-Criado A. Imaging of HCC. Abdom Imaging 2012;37:215-30.
5. Sundaram M, McGuire MH, Herbold DR. Magnetic resonance imaging of soft tissue masses: an evaluation of fifty-three histologically proven tumors. Magn Reson Imaging 1988;6:237-48.
6. Halavaara J, Breuer J, Ayuso C, et al. Liver tumor characterization: comparison between liver-specific

gadoxetic acid disodium-enhanced MRI and biphasic CT--a multicenter trial. J Comput Assist Tomogr 2006;30:345-54.
7. Kreft BP, Muller-Miny H, Sommer T, et al. Diagnostic value of MR imaging in comparison to CT in the detection and differential diagnosis of renal masses: ROC analysis. Eur Radiol 1997;7:542-7.
8. Lambin P, Rios-Velazquez E, Leijenaar R, et al. Radiomics: extracting more information from medical images using advanced feature analysis. Eur J Cancer 2012;48:441-6.
9. Parekh V, Jacobs MA. Radiomics: a new application from established techniques. Expert Rev Precis Med Drug Dev 2016;1:207-26.
10. Li Z, Mao Y, Huang W, et al. Texture-based classification of different single liver lesion based on SPAIR T2W MRI images. BMC Med Imaging 2017;17:42.
11. Yu JY, Zhang HP, Tang ZY, et al. Value of texture analysis based on enhanced MRI for predicting an early therapeutic response to transcatheter arterial chemoembolisation combined with high-intensity focused ultrasound treatment in hepatocellular carcinoma. Clin Radiol 2018;73:758.e9-758.e18.
12. Zhou W, Zhang L, Wang K, et al. Malignancy characterization of hepatocellular carcinomas based on texture analysis of contrast-enhanced MR images. J Magn Reson Imaging 2017;45:1476-84.
13. Aerts HJ, Velazquez ER, Leijenaar RT, et al. Decoding tumour phenotype by noninvasive imaging using a quantitative radiomics approach. Nat Commun 2014;5:4006.
14. Zhao B, Tan Y, Tsai WY, et al. Reproducibility of radiomics for deciphering tumor phenotype with imaging. Sci Rep 2016;6:23428.
15. Moteki T, Horikoshi H. Evaluation of hepatic lesions and hepatic parenchyma using diffusion-weighted echo-planar MR with three values of gradient b-factor. J Magn Reson Imaging 2006;24:637-45.
16. Nasu K, Kuroki Y, Nawano S, et al. Hepatic metastases: diffusion-weighted sensitivity-encoding versus SPIO-enhanced MR imaging. Radiology 2006;239:122-30.
17. Kierans A, Bennett G, Mussi T, et al. Characterization of malignancy of adnexal lesions using ADC entropy: comparison with mean ADC and qualitative DWI assessment. J Magn Reson Imaging 2013;37:164-71.
18. Wibmer A, Hricak H, Gondo T, et al. Haralick texture analysis of prostate MRI: utility for differentiating non-cancerous prostate from prostate cancer and differentiating prostate cancers with different Gleason scores. Eur Radiol 2015;25:2840-50.
19. Wurnig MC, Donati OF, Ulbrich E, et al. Systematic analysis of the intravoxel incoherent motion threshold separating perfusion and diffusion effects: Proposal of a standardized algorithm. Magn Reson Med 2015;74:1414-22.
20. Muhi A, Ichikawa T, Motosugi U, et al. High-b-value diffusion-weighted MR imaging of hepatocellular lesions: estimation of grade of malignancy of hepatocellular carcinoma. J Magn Reson Imaging 2009;30:1005-11.
21. Chandarana H, Taouli B. Diffusion-weighted MRI and liver metastases. Magn Reson Imaging Clin N Am 2010;18:451-64, x.
22. Shafiq-Ul-Hassan M, Zhang GG, Latifi K, et al. Intrinsic dependencies of CT radiomic features on voxel size and number of gray levels. Med Phys 2017;44:1050-62.
23. Karlik SJ. Exploring and summarizing radiologic data. AJR Am J Roentgenol 2003;180:47-54.
24. Hunter LA, Krafft S, Stingo F, et al. High quality machine-robust image features: identification in nonsmall cell lung cancer computed tomography images. Med Phys 2013;40:121916.
25. Lin LI. A concordance correlation coefficient to evaluate reproducibility. Biometrics 1989;45:255-68.
26. Nasu K, Kuroki Y, Tsukamoto T, et al. Diffusion-weighted imaging of surgically resected hepatocellular carcinoma: imaging characteristics and relationship among signal intensity, apparent diffusion coefficient, and histopathologic grade. AJR Am J Roentgenol 2009;193:438-44.
27. Choi IY, Lee SS, Sung YS, et al. Intravoxel incoherent motion diffusion-weighted imaging for characterizing focal hepatic lesions: Correlation with lesion enhancement. J Magn Reson Imaging 2017;45:1589-98.
28. Koh DM, Collins DJ. Diffusion-weighted MRI in the body: applications and challenges in oncology. AJR Am J Roentgenol 2007;188:1622-35.

Cite this article as: Zhang J, Qiu Q, Duan J, Gong G, Jiang Q, Sun G, Yin Y. Variability of radiomic features extracted from multi-b-value diffusion-weighted images in hepatocellular carcinoma. Transl Cancer Res 2019;8(1):130-140. doi: 10.21037/tcr.2019.01.14

